PCCP

Accepted Manuscript

ROYAL SOCIETY OF CHEMISTRY

www.rsc.org/pccp

Journal Name

ARTICLE

Nanostring-cluster hierarchical structured Bi_2O_3: synthesis, evolution and application in biosensing

Received 00th January 20xx,
Accepted 00th January 20xx

DOI: 10.1039/x0xx00000x

www.rsc.org/

Ya-Nan Yu, Shi-Yu Lu, Shu-Juan Bao*, Qiang-Qiang Sun, Sheng-Hui Liao

In this work, a simple strategy was developed to fabricate a new Bi_2O_3 nanostring-cluster hierarchical structure. Precursor microrods composed of $Bi(C_2O_4)OH$ were initially grown under hydrothermal conditions. After calcination in air, $Bi(C_2O_4)OH$ microrods were carved into unique string-cluster structures by the gas produced during the decomposition process. In order to explain the formation mechanism, the effects of pyrolysis temperature and time on the morphology of as-prepared samples were investigated and discussed in detail. It was discovered that the nanostring-cluster structured Bi_2O_3 consists of thin nanoplatelet arrays, which is advantageous for glucose enzyme immobilization and designing biosensors. The resulting Bi_2O_3 structure showed excellent capability in the modification of electrode surfaces in biosensors by enhancing sensitivity, good specificity, and response time. Such qualities of a biosensor are ideal characteristics for glucose sensing performance and allow for further explorations of its application in other fields.

Introduction

It is well known that the physical and chemical properties of materials, including morphology, size, and surface-to-volume ratio, are strongly dependent on their microstructures.[1-4] Therefore, the synthesis of inorganic nanomaterials with controllable morphology, dimensionality, and orientation is highly desirable so that they can be used according to their unique and promising properties.[5, 6] Specifically, the ordered hierarchical structure made up of two-dimensional (2D) building blocks has been a large center of focus due to its important role in the systematic study of structure-property relationships and improved physical and chemical properties.[7-10] However, how to effectively build a unique ordered hierarchical structure is still a great challenge.

Recently, bismuth-containing nanostructures, such as Bi_2O_3[11-13], $(BiO)_2CO_3$[14-16], BiOCl[17-20] and Bi_2S_3[21, 22] with desirable morphologies have stimulated extensive research interest, owing to their broad applications in the fields of electronics, biomedicine, and environmental sciences. Among these bismuth-containing nanostructures, β-Bi_2O_3 single crystalline was commonly used as a precursor and template to build various superstructures. For example, Qian Liu *et al.* synthesized BiOCl nanowire with a casement-like hierarchical structure by dipping β-Bi_2O_3 nanowire in HCl solution, which was further transformed the ordered BiOCl superstructures into nested self-similar networks of Bi_2S_3 with the presence of S^{2-}.[23] Liu also fabricated $(BiO)_2CO_3$ orthogonal networks by incubating β-Bi_2O_3 film in a blended solution of $NaHCO_3$ and HNO_3. The authors believe such networks are explained by the unique structure of β-Bi_2O_3, which has two equivalent perpendicular facets, (220) and (2-20). Hence, either the *c*- or the (110)-axis out of plane can lead to the formation of 2D orthogonal networks with mutually perpendicular woven nanowalls. Inspired by the above reports, the crystal structure of the precursor in this work is aimed to have a great influence on the morphology of the corresponding products.[24] However, we wonder if this will offer us a chance to enrich novel nanomaterials by choosing raw materials with certain crystal structure features or to prepare hierarchical structured materials using more simple methods.

The materials with hierarchical structure are regarded as one of the most promising materials to play an increasingly important role in remission of environmental and energy crises[25-27], and also has brought a great momentum to bioelectroanalysis in recent years[28]. In this work, a unique hierarchical structured Bi_2O_3 nanostring-cluster was constructed by initially decomposing bismuth oxalate rods. The hierarchical nanostring-cluster structure was constituted by thin nanoplatelet arrays, and the gaps between these nanoplatelets provided an appropriate position for immobilizing enzyme. Thus, the as-prepared materials were explored based on their capability to modify electrodes and

Institute for Clean Energy & Advanced Materials, Faculty of Materials and Energy, Southwest University, Chongqing, 400715, P. R. China. E-mail:baoshj@swu.edu.cn

fabricate enzymatic biosensors. Using immobilization of glucose oxidase (GOD), our designed glucose sensor exhibits outstanding glucose sensing performance, including excellent sensitivity, good specificity, and fast response. Based on the experimental results in this work, we proposed a formation mechanism to offer physicochemical insights for future explorations on the novel properties of unique nanostructures as potential, functional materials in important applications.

Experimental

Materials synthesis

In a typical procedure, 1.5 g of oxalic acid, $H_2C_2O_4$, was dissolved in 30 mL deionization (DI) water. 250 mg of bismuth nitrate pentahydrate, $Bi(NO_3)_3{\cdot}5H_2O$, was added into the oxalic acid solution. After stirring for 20 min, the resulting solution was transferred into an autoclave and then heated at 180°C for 14 h. When it was cooled down to room temperature, the gray precipitate was obtained by centrifugation. After rinsing with DI water and ethanol, the precipitate was dried at 80°C in a vacuum oven overnight. The obtained powder was named BiCH, which was then annealed at 250, 280, and 350°C for 2 h. Their products were donated as BiCH-250, BiCH-280, and BiCH-350.

Material characterizations

The crystal structures of the prepared samples were characterized by X-ray diffraction (XRD, Shimadzu XRD-7000). The morphology and microstructure of the prepared samples were observed by transmission electron microscopy (TEM, JEM-2100), field emission scanning electron microscopy (FESEM, JEOL-7800F). The X-ray photoelectron spectroscopy (XPS) data were obtained by a spectrometer (Escalab 250xi, Thermo Scientific). The thermal properties of the synthesized precursors were studied by a Thermo Gravimetric Analyzer (TGA, Q50, USA) in N_2 atmosphere.

Electrochemical characterizations

Glassy carbon electrodes with 3 mm in diameter (GCE, CH Instruments) were polished with 0.3 and 0.05 μm alumina powder, followed by thorough rinsing with deionized water. After sonicating in 1 M nitric acid, acetone and deionized water, and then dried naturally. Subsequently, the electrode was modified with chitosan by electrodeposition in a 0.2% chitosan solution at −2.5 V for 10 seconds to form a positively charged surface. The modified GCE was prepared by a simple casting method. Protein immobilization was achieved by immersing 2 mg of as-prepared samples in 100 μl of distilled water under ultra-sonication. After that 1 mg GOD was added into the above suspension, which was shaken for 30 min and then stored at 4 ℃ for 2 day for protein adsorption. The bioconjugates obtained above were re-shaken and 5 μl of this suspension was deposited on the center of the pretreated GCE. Then the electrodes were left to dry at room temperature, after which 10 μl of 0.5% Nafion were subsequently placed on the whole of the electrode surface to form a Nafion membrane. The electrochemical measurements were carried out using a three-electrode system, employing a platinum wire as the counter electrode, a Ag/AgCl electrode as the reference, and different samples modified glass carbon electrode (GCE) as the working electrode.

Results and discussion

Figure 1a shows the typical XRD patterns of the precursor used in this work and the sample obtained by annealing at 280°C for 2 h. The diffraction peaks of the precursor can be indexed to $Bi(C_2O_4)OH$, which matched well with results reported by Wang *et al*.[11] After annealing at 280°C for 2 h, the characteristic peaks of $Bi(C_2O_4)OH$ disappeared, and new diffraction peaks appeared. It is worth noting that those peaks index to a combination of β-Bi_2O_3 (PDF no.74-1374), α-Bi_2O_3 (PDF no.71-0465).[13, 29] Figure 1b1 shows the FESEM image of the precursor, which consisted of 1μm long rods with smooth surfaces. After annealing at 280°C for 2 h, the resultant product was very different from its precursor, as shown in Figure 1b2. The image of BiCH-280 shows a unique hierarchical structure consisting of an array of thin nanoplatelets. Details of the structures can be further observed *via* high-magnification FESEM and TEM images (Figures 1c1 to c3), which illustrate very ordered, nanostring cluster hierarchical structures with many gaps generated between very thin nanoplatelets. In order to understand the formation mechanism of these unique super-structures, more experiments were carried out.

Journal Name

ARTICLE

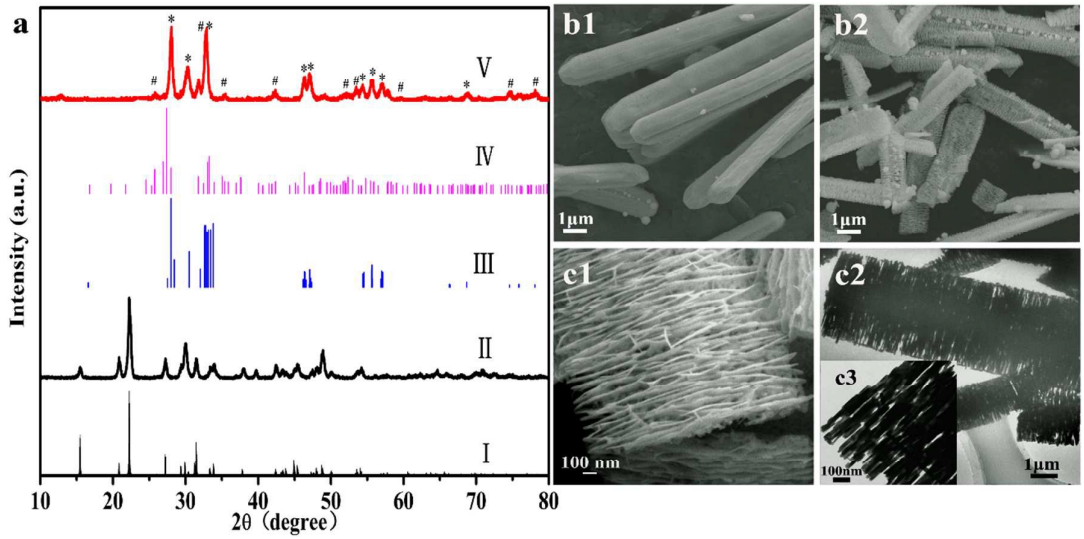

Figure 1. XRD patterns of the as-synthesized samples: (a) I-standard patterns of $Bi(C_2O_4)OH$; II-BiCH; III-standard pattern of β-Bi_2O_3; IV-standard pattern of α-Bi_2O_3; V-BICH-280 ('*' stands for the characteristic peak of β-Bi_2O_3, '#' stands for the characteristic peak of α-Bi_2O_3). (b1) Low-magnification SEM of BiCH and (b2) BiCH-280. (c1) High-magnification SEM and (c2-3) TEM of BiCH-280 sample.

The thermal properties of the precursor were studied using TG-DSC analysis, and results are displayed in Figure 2. An obvious weight loss of 23.4% appeared between 250°C and 350°C, which is due to the decomposition of precursor and the formation of a new phase. After analyzing the DSC curve, it was determined that the crystal phase transformation temperature was around 280°C. When the temperature was greater than 350°C, no obvious change is observed from the curve, an indication that a stable structure had formed at this stage. Hence, in this work 250, 280, and 350°C were selected as the temperatures to study the effects of annealing on the microstructure and morphology of the products.

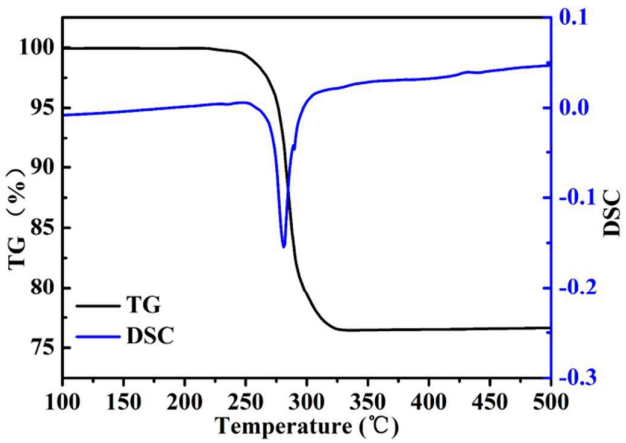

Figure 2. TG-DSC curve of the precursor.

The XRD patterns of the samples obtained at different temperatures are shown in Figure 3. As the temperature increases, the major peaks of the precursor gradually weaken and then finally disappear, and meanwhile, several new

characteristic peaks occur.The sample obtained at 250°C is a compound consisting of $Bi(C_2O_4)OH$ and β-Bi_2O_3. When the annealing temperature increases to 350°C, all of the XRD peaks of the sample are assigned to α-Bi_2O_3, which is in good accordance with the standard spectrum (PDF card 71-0465). This result indicates that annealing at 350°C for 2 h is favorable for the complete formation of α-Bi_2O_3. Subsequently, the morphologies of the samples obtained at different temperatures were observed by FESEM. As shown in Figures 3b to 3e, it is clear that all the samples remain in a 1D rod structure of their precursor. After annealed at 250°C for 2 h, few thin nanoplatelets begin to emerge vertically on the surface, which can be seen in Figure 4b. When the temperature increases to 350°C, the nanoplatelet structures are destroyed, and big particles connect together to form nanoporous structured rods.

In order to fully understanding the formation mechanism of the unique super-structures obtained at 280°C, the effect of reaction time on the microstructure of products was further considered. Figure 4 exhibits the morphology evolution of the products obtained at the same annealing temperature with variations in the reaction time. It is clear that the morphology of nanoplatelets occurs in a short time of 30 min. After prolonging the reaction time, the countless nanoplatelet arrays grew along the axial direction of the rods. An increasing amount of gaps between the nanoplatelets appeared, and the smooth surface gradually faded away. It is worth noting that the super-structure did not change much even after being annealed for 12 h. Although the gaps between nanoplatelets became narrower, the integral structures did not change. The time dependent experiments indicate that the typical structure is formed through a decomposition process.

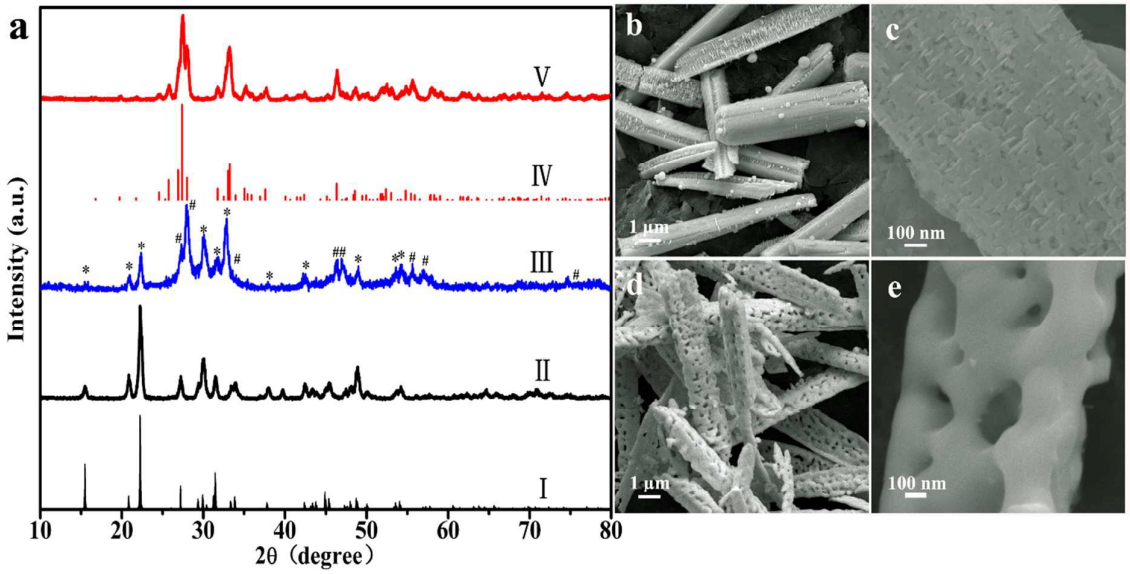

Figure 3. XRD of the standard pattern of the samples: (a) I. standard patterns of $Bi(C_2O_4)OH$; II. BiCH; III. BICH-250 ('*' stands for the characteristic peak of $Bi(C_2O_4)OH$, '#' stands for the characteristic peak of β-Bi_2O_3); IV. standard pattern of α-Bi_2O_3; V-BICH-350. (b, c) FESEM of BiCH-250; (d, e) BiCH-350.

Journal Name

ARTICLE

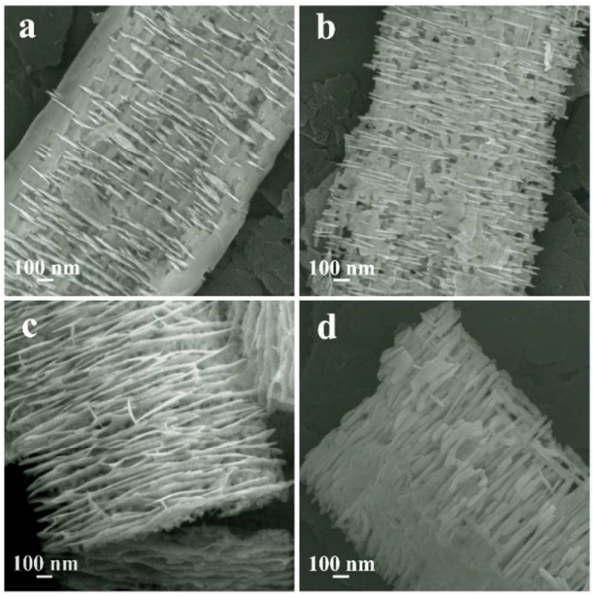

Figure 4. FESEM of BiCH calcined at 280°C for (a) 30, b) 60, c) 120, and d) 720 min.

Further structural details and compositions of the samples obtained at different temperatures were explored by XPS analysis. A typical XPS survey spectrum of O 1s is presented in Figure 5. All of the O 1s peaks consist of three peaks. The peak at 528.1 eV can be ascribed to the oxygen attached to the Bi–O bond, while the other two peaks at 529.4 eV and 530.6 eV can be assigned to the OH and CO_3 species, respectively. [14, 30, 31] Considering the four XPS spectra, there is a tendency for the ratio of those three peaks to change with increasing temperature. The content of Bi–O increased with the increasing annealing temperature, indicating that the $Bi(C_2O_4)OH$ is transferring to Bi_2O_3.

It is generally believed that a crystal habit is responsible for the final crystallographic phase of the products.[32, 33] A crystal will always grow in the direction of some preferred orientation.[34] The BiCH has a layered Bi_2O_2 structure interleaved by double layers of a carboxyl group,[35] which may result in the morphology of thin nanoplatelets. However, it is worth noting that the morphology of products is also closely related with annealing temperature. It is well known that the precursor, $Bi(C_2O_4)OH$, will decompose to Bi_2O_3, H_2O, CO_2, and CO gases in the presence of high temperatures. The generated gas acts as a "knife" to carve the morphology of products. As expected, when the pyrolysis temperature was 280°C, the decomposed gases "carved" rods into the nanostring-cluster hierarchical structures slowly. When the temperature increased to 350°C, the decomposed gas flows out quickly, and the porous structure along the rods formed instead of nanostring-cluster hierarchical structures. This occurrence indicates that the decomposition rate also has a great influence on the morphology of products.

With the development of nanoscience and nanotechnology, more and more nanomaterials are being used to modify biosensor electrodes and boost the fast development of bioelectroanalysis.[36] The nanostring-cluster hierarchical structures constituted by thin nanoplatelets may be a good supporting material for the immobilization of glucose oxidase (GOD) and provide fast ionic channels for electrocatalytic processes. Hence, in this work, the as-prepared superstructures were used as electrode modifying materials to study the process-structure-property relationship in nanomaterial synthesis and their application in biosensors.

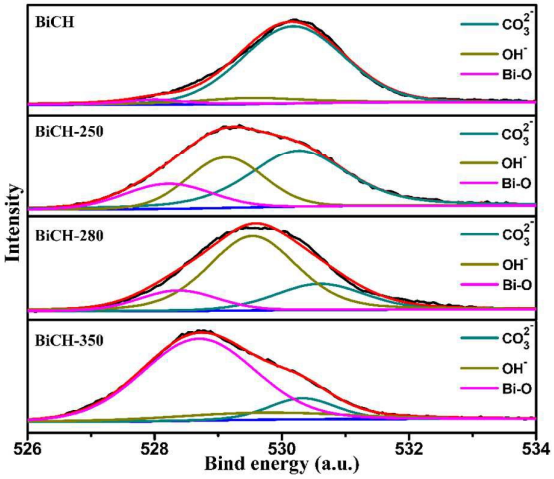

Figure 5. XPS of O in different samples.

Cyclic voltammetry (CV) was employed to evaluate the performance of the fabricated biosensor. The direct electrochemistry of GOD immobilized on a modified glassy

carbon electrode (GCE) was investigated in 0.1 M, pH 7, N_2-saturated PBS solutions at 100 mV s^{-1}, which is from the flavin adenine dinucleotide (FAD) of GOD. As shown in Figure 6a, no redox peaks were observed for either the bare electrode or the GOD-modified electrode, suggesting that they are electrochemically silent in the potential range. A pair of weak redox peaks can be seen for the GOD@BiCH-250 and GOD@BiCH-350 modified electrodes, while a couple of well-defined and nearly symmetrical strong redox peaks were observed for the GOD@BiCH-280 modified electrode. The latter demonstrates that the BiCH-280 can effectively immobilize GOD, providing it with excellent direct electron transfer capability due to its unique superstructure and possible physical adsorption. Figure 6c displays the cyclic voltammograms of the GOD@BiCH-280 modified GCEs in N_2- and air-saturated 0.1 M PBS solution. As reported in previous literature, in the presence of oxygen, the reduced enzyme (GOD-$FADH_2$) can be further oxidized by

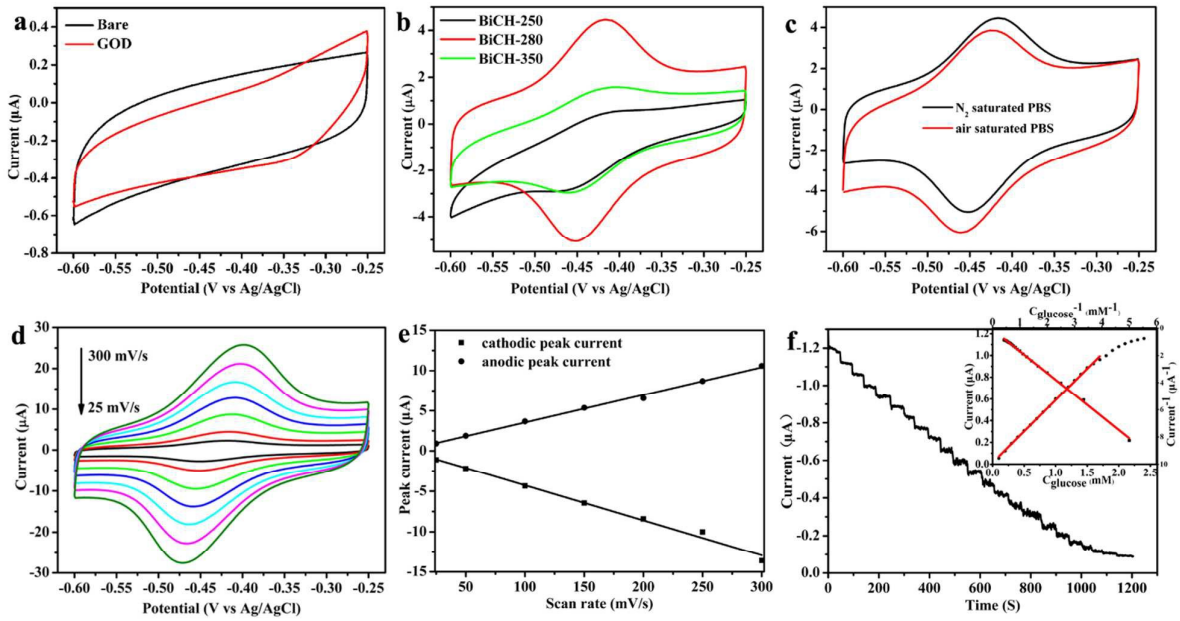

Figure 6. (a) CVs of GCE and GOD modified GCE in 0.1 M, pH 7 PBS solution at different scan rates from 25 to 300 mV s^{-1}. (b) CVs of different samples immobilize GOD. (c) CVs of BiCH-280/GOD in N_2-saturated and air-saturated. (d) CVs of GOD@BiCH-280 at different scan rates. (e) Plots of peak currents versus scan rate. (f) Typical steady state response of the biosensor on successive injection of 0.1 mmol glucose solution into 0.1 M, pH 7 N_2-saturated PBS solution while stirring at an applied potential of -0.4 V. The inset is the calibration curve of sensor.

dissolving oxygen very quickly at the surface of the electrode. Hence, the cathodic peak current is larger, and the anodic peak is lower in the air-saturated solution as compared to the corresponding peak in the N_2-saturated PBS solution. In other words, the electrochemically formed GOD-$FADH_2$ can electrocatalyze the reduction of dissolved oxygen. To evaluate the reversible electron transfer phenomenon of the GOD@BiCH-280 modified electrode in more detail, the CVs at different scan rates were recorded in 0.1 M, pH 7.0 PBS solution. As shown in Figure 6d, with the scan rate increasing, the cathodic and anodic peak currents linearly rise simultaneously in the range of 25~300 mVs^{-1}, indicating a surface controlled electrochemical oxidation/reduction of the $FAD/FADH_2$ involved in the GOD-structure. In order to investigate the bioactivity of the adsorbed GOD, the fabricated electrode was employed to detect glucose. Figure 6f shows a typical current-time plot for the BiCH-280/GOD modified electrode on successive injections of a glucose solution into N_2-saturated and stirred 0.1 M, pH 7.0 PBS solutions at -0.4 V. Each successive addition of glucose resulted in an increase in the steady state current. The peak current of the BiCH-280/GOD modified electrode increased linearly with increasing concentrations of glucose that ranged from 0.1 mM to 1.7 mM, with a correlation coefficient of 0.996 and sensitivity of 8.15 μA mM^{-1} cm^{-2}. A low detection limit of 48.4 μM was also readily achieved at a signal-to-noise ratio of 3. The calibration plot in the inset of Figure 6f shows well-defined, typical behavior of an enzymatic kinetic reaction. The apparent Michaelis-Menten constant (K_M), as an indicator of enzyme-substrate reaction kinetics, can be used to evaluate the biological activity of the immobilized enzyme, which was calculated to be 15.74 mM (R=0.998) according to the Lineweaver-Burk equation reported in previous literature.[37] The low value of K_M indicates that BiCH-280 can provide a

favorable microenvironment for GOD to retain its bioactivity and achieve direct electron transfer. The stability of the GOD@BiCH-208 modified electrode was also estimated in our work. When the biosensor was stored at 4 °C in dry state and measured every three day, the current response for glucose decreased by only about 11 % of the original value after two weeks. There is also no obvious response current difference among five electrodes prepared at same condition. The good stability and reproducibility of the biosensor may be attributed to the unique hierarchical structure of Bi_2O_3 nanostring-cluster.

Conclusions

In this featured work, we demonstrated a simple approach to synthesize hierarchical nanostring-cluster structures of Bi_2O_3 constructed by nanoplate subunits *via* a decomposition process. The unique structure of Bi_2O_3 nanostring-cluster exhibits great potential in adsorption, immobilizing enzymes, catalysis, and advanced electrochemical energy storage systems. As an example, the resultant BiCH-280 manifests excellent biosensing performance when evaluated as an electrode modifying material for glucose detection. Further research to disclose the mystery of its formation mechanism is currently in progress, particularly to understand its application in the field of photocatalysis.

Acknowledgements

This work is financially supported by National Natural Science Foundation of China (21163021 and 21375108); Chongqing Key Laboratory for Advanced Materials and Technologies of Clean Energies; Natural Science Foundation of Chongqing (cstc2013jcyjA5004); Program for Excellent Talents in Chongqing (102060-20600218).

Notes and references

1. X. Duan, Y. Huang, Y. Cui, J. Wang and C. M. Lieber, *Nature*, 2001, **409**, 66-69.
2. Y. Xia, P. Yang, Y. Sun, Y. Wu, B. Mayers, B. Gates, Y. Yin, F. Kim and H. Yan, *Advanced materials*, 2003, **15**, 353-389.
3. H. G. Yang and H. C. Zeng, *Angewandte Chemie*, 2004, **116**, 6056-6059.
4. S. Song, Y. Zhang, J. Feng, Y. Xing, Y. Lei, W. Fan and H. Zhang, *Crystal Growth and Design*, 2008, **9**, 848-852.
5. H. Spillmann, A. Dmitriev, N. Lin, P. Messina, J. V. Barth and K. Kern, *Journal of the American Chemical Society*, 2003, **125**, 10725-10728.
6. H. Yan, R. He, J. Johnson, M. Law, R. J. Saykally and P. Yang, *Journal of the American Chemical Society*, 2003, **125**, 4728-4729.
7. Y.-F. Hou, S.-J. Liu, J.-h. Zhang, X. Cheng and Y. Wang, *Dalton Transactions*, 2014, **43**, 1025-1031.
8. M. Safdar, Z. Wang, M. Mirza, F. K. Butt, Y. Wang, L. Sun and J. He, *Journal of Materials Chemistry A*, 2013, **1**, 1427-1432.
9. J.-L. Mi, N. Lock, T. Sun, M. Christensen, M. Søndergaard, P. Hald, H. H. Hng, J. Ma and B. B. Iversen, *ACS nano*, 2010, **4**, 2523-2530.
10. Y. Peng, M. Yan, Q.-G. Chen, C.-M. Fan, H.-Y. Zhou and A.-W. Xu, *Journal of Materials Chemistry A*, 2014, **2**, 8517-8524.
11. H. Wang, H. Yang and L. Lu, *RSC Adv.*, 2014, **4**, 17483-17489.
12. X. Gou, R. Li, G. Wang, Z. Chen and D. Wexler, *Nanotechnology*, 2009, **20**, 495501.
13. Y. Qiu, M. Yang, H. Fan, Y. Zuo, Y. Shao, Y. Xu, X. Yang and S. Yang, *CrystEngComm*, 2011, **13**, 1843-1850.
14. P. Madhusudan, J. Zhang, B. Cheng and G. Liu, *CrystEngComm*, 2013, **15**, 231-240.
15. H. Cheng, B. Huang, K. Yang, Z. Wang, X. Qin, X. Zhang and Y. Dai, *ChemPhysChem*, 2010, **11**, 2167-2173.
16. H. Huang, J. Wang, F. Dong, Y. Guo, N. Tian, Y. Zhang and T. Zhang, *Crystal Growth & Design*, 2015, **15**, 534-537.
17. K. Shen, M. Gondal, A. Al-Saadi, L. Li, X. Chang and Q. Xu, *Research on Chemical Intermediates*, 2015, **41**, 2753-2766.
18. Y. Mi, L. Wen, Z. Wang, D. Cao, Y. Fang and Y. Lei, *Applied Catalysis B: Environmental*, 2015, **176**, 331-337.
19. L. Ding, R. Wei, H. Chen, J. Hu and J. Li, *Applied Catalysis B: Environmental*, 2015, **172**, 91-99.
20. S. Weng, J. Hu, M. Lu, X. Ye, Z. Pei, M. Huang, L. Xie, S. Lin and P. Liu, *Applied Catalysis B: Environmental*, 2015, **163**, 205-213.
21. G. Chen, Y. Yu, K. Zheng, T. Ding, W. Wang, Y. Jiang and Q. Yang, *Small*, 2015.
22. J. Andzane, G. Kunakova, J. Varghese, J. Holmes and D. Erts, *Journal of Applied Physics*, 2015, **117**, 064305.
23. C. F. Guo, S. Cao, J. Zhang, H. Tang, S. Guo, Y. Tian and Q. Liu, *Journal of the American Chemical Society*, 2011, **133**, 8211-8215.
24. C. F. Guo, J. Zhang, Y. Tian and Q. Liu, *Acs Nano*, 2012, **6**, 8746-8752.
25. M. Muruganandham, R. Amutha, G.-J. Lee, S.-H. Hsieh, J. J. Wu and M. Sillanpää, *The Journal of Physical Chemistry C*, 2012, **116**, 12906-12915.
26. F.-L. Zheng, G.-R. Li, Y.-N. Ou, Z.-L. Wang, C.-Y. Su and Y.-X. Tong, *Chemical Communications*, 2010, **46**, 5021-5023.
27. H. Xu, X. Hu, H. Yang, Y. Sun, C. Hu and Y. Huang, *Advanced Energy Materials*, 2015, **5**.
28. R. Jain and R. Sharma, *Journal of Applied Electrochemistry*, 2012, **42**, 341-348.
29. Y. Yan, Z. Zhou, Y. Cheng, L. Qiu, C. Gao and J. Zhou, *Journal of Alloys and Compounds*, 2014, **605**, 102-108.
30. S. D. Gardner, C. S. Singamsetty, G. L. Booth, G.-R. He and C. U. Pittman, *Carbon*, 1995, **33**, 587-595.
31. F. Dong, Y. Sun, M. Fu, W.-K. Ho, S. C. Lee and Z. Wu, *Langmuir*, 2011, **28**, 766-773.
32. J. Xiong, G. Cheng, Z. Lu, J. Tang, X. Yu and R. Chen, *CrystEngComm*, 2011, **13**, 2381-2390.

33. M. Rivenet, P. Roussel and F. Abraham, *Journal of Solid State Chemistry*, 2008, **181**, 2586-2590.
34. S. Cong, T. Sugahara, T. Wei, J. Jiu, Y. Hirose, S. Nagao and K. Suganuma, *Cryst. Growth Des.*, 2015.
35. J. He, W. Y, F. Y, Q. X, Z. Z, L. Q, T. WS, G. CL, Z. H and C. H, *Acs Nano*, 2013, **7**, 2733-2740.
36. S. J. Bao, C. M. Li, J. F. Zang, X. Q. Cui, Y. Qiao and J. Guo, *Advanced Functional Materials*, 2008, **18**, 591-599.
37. B. K. Hamilton, C. R. Gardner and C. K. Colton, *AIChE Journal*, 1974, **20**, 503-510.